A Novel Airbag Aided Differential-drive Capsule Robot Towards Colonoscopy

Jianlin Yang (yangjianlin@nuaa.edu.cn)

NUAA College of Aerospace Engineering: Nanjing University of Aeronautics and Astronautics College of Aerospace Engineering https://orcid.org/0000-0003-4555-9687

Zhijun Sun

Nanjing University of Aeronautics and Astronautics

Yu Guo

Jinling Institute of Technology

Research Article

Keywords: soft robot, wheeled robot, colonoscopy, force control

Posted Date: June 22nd, 2022

DOI: https://doi.org/10.21203/rs.3.rs-1651133/v1

A novel airbag aided differential-drive capsule robot towards colonoscopy

Jianlin YANG[1] (yangjianlin@nuaa.edu.cn)
Zhijun SUN[1]* (Corresponding author, meezjsun@nuaa.edu.cn)
Yu GUO[2] (guoyu0834@163.com)

Abstract Colorectal cancer is the third most common cancer in the world, which is a serious threat to human health. Endoscopy is the most effective way to screen colorectal cancer. However, it is very difficult to design a robot that can move in a complex colon. Soft robots can adapt to a variety of unstructured environments, and their interaction with humans is more secure. This paper presents a novel differential-drive caterpillar-based robot for colonoscopy, which is expanded by an airbag. Combining the advantages of the soft robot and the wheeled robot, the robot has both the flexibility of the former and the rapidity of the latter. The size of the robot in the contraction state is only ϕ28mm × 35mm and the length of traction module is only 28mm. The robot can be expanded to a diameter of 50mm and has a maximum speed of 5mm/s. The design concept of the robot and its traction module are described in detail. To ensure the stable movement of robot, the controlled output force of the robot caterpillar track is tested by experiments. In addition, the robot is placed in a curved bellow to move, and its motion validity is verified.

Keywords soft robot, wheeled robot, colonoscopy, force control

1 Introduction

Colorectal cancer ranks third among the most commonly diagnosed cancers in the world, which is seriously harmful to human health [1]. Because of its unique advantages, endoscopy is the main diagnostic method of colorectal cancer [2]. Flexible colonoscopy is the most widely used, which can clearly see the focus and can perform biopsy operations or even surgeries. However, for doctors, colonoscopy is a challenging operation, which may be related to low completion rate, serious complications and unpleasant experience of patients. And it also often causes some problems, such as bleeding, perforation, incomplete examination, failure in inserting the endoscopy and other risks. Capsule endoscopy is a new technology in recent years [3]. Although the examination process is noninvasive and painless, it can not stay in the intestine, and the detection rate in the colon segment is low, and the price is expensive. It can not be used in large-scale clinical practice, nor can it carry out biopsy operation.

In view of the above problems, many research institutions in the world have carried out innovative colon inspection research, and the research focus is mainly on the new active motion endoscope and intelligent diagnosis. Especially the former, a lot of useful modes of motion have been carried out, such as caterpillar track or wheel type [4-9], legged type [10-11], barb type [12-14], inchworm type [15-20], peristaltic type [21-22] and other methods [23-26]. However, due to the difficulty of miniaturization design and harsh application situation, there is no active-locomotion endoscopy in clinical application. But even so, soft robot is the most promising application in colon inspection.

In recent years, due to safety of flexible structure, soft robot has attracted the attention of many researchers. Using double inflated balloon and imitating inchworm Luigi Manfredi developed an active motility colonoscope, which showed good motility [15]. However, the inchworm robot's movement is intermittent, and due to the scalability and mucosity of the intestine, its forward efficiency is relatively low. According to the previous literature, wheeled robot has high efficiency. Nevertheless, the past wheeled or crawler colon inspection robots are mainly divided into two categories. One is a single motor as the driving source to drive multiple tracks [4-5]. The robot has a simple and compact structure,

but it has few active degrees of freedom, so it can't turn actively and pass through the complex environment of colon. The other also has multiple tracks and is driven by multiple motors[6-8]. The robot can turn and even unfold to adapt to the size of the intestine. However, the mechanical structure of this kind of robot is complex and usually has a large size.

The concept of zero-volume actuation is very suitable for the compact design of robot. According to this, R. F. Natividad designed a caterpillar robot with compact structure [27]. Wyatt Felt designed and manufactured a pneumatic bending actuator with excellent performance by using folded tube [28]. Based on the concept of zero-volume actuation, this paper proposes a caterpillar-based capsule robot expanded by an airbag for colonoscopy. The robot is driven by three independent traction modules, and each traction module is driven by one motor which drives the worm gears. The three traction modules can be driven by a constrained airbag expansion to adapt to the changing intestinal diameter. So this robot has both the safety of flexible robots and the high efficiency of wheeled robots. This article describes the design concept and details of the robot. The kinematics model and the statics model based on empirical data is established. They are used to control the motion and the output force of the robot, and good force control effect is obtained. The robot can move forward and turn in a curved bellows. The contributions of this paper are as follows.

(1) A novel capsule robot for colonoscopy is proposed, which has not only the flexibility of a soft robot, but also the speed of a wheeled robot.

(2) The output force of the robot caterpillar tracks can be controlled in a certain range based on the established statics model, which can ensure the safety and stability of the robot.

(3) The motion effectiveness of the robot is verified in a curved bellows. And its speed and traction force meet the requirements.

2 Robot system

2.1 Design considerations

The human colon consists of five parts: ascending colon, transverse colon, descending colon, sigmoid colon, rectum and cecum [29]. Its diameter is between 3.32cm and 4.91cm, and its length is about 129.54cm. The colon not only has a variable diameter, but also has several large angle bends. In addition, the inner surface of the colon is slippery and has many folds. So the robot should have enough dexterity. Specifically, the robot should have four degrees of freedom: forward and backward along the intestinal center line, turn around two directions orthogonal to the forward direction, and expand to adapt to the size of the intestinal tract. The inner wall of the colon is soft and fragile. Accidents may occur in common colonoscopy operation, such as bleeding and perforation. Therefore, we should ensure that the robot has certain safety, sharp parts can not be exposed, and the force between robot and intestinal wall should be kept in a certain range. A colonoscopy operation takes about 20 to 30 minutes, and it takes about 8 minutes to pass through the entire colon [30,31]. Hence the forward speed of colonoscopy robot should not be lower than that of conventional colonoscopy. The conventional colonoscopy also has the functions of lighting, water insufflation and gas insufflation, biopsy and so on. Consequently, the robot should have these functions as far as possible. In addition to the above requirements, the design and manufacture of robots should also consider the cost, because the high price will make people with poor economic conditions unable to bear.

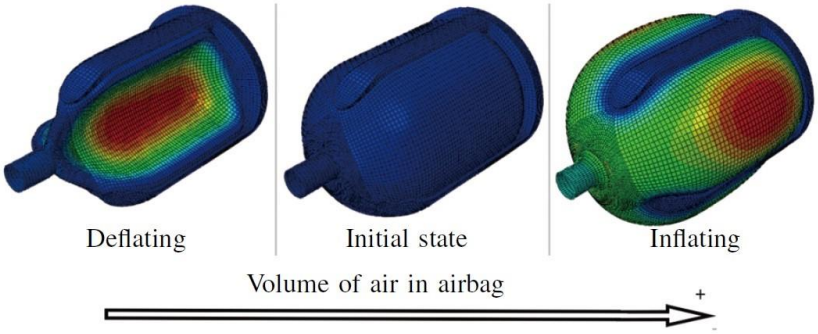

Fig. 1 Three ABAQUS simulation diagrams of the designed airbag with the internal pressure from small to large (-5kPa to 30kPa).

2.2 Design of the robot

High-efficiency wheeled robot for colon inspection must have four active degrees of freedom, namely one forward and backward, two steering degrees of freedom and one expansion. There are many ways to achieve this goal. Pure machinery is one method. However, it is difficult to miniaturize because of its high cost. And strain gauges are needed to detect the contact force between robot and intestinal wall. The airbag can be driven by zero volume and has good safety. The force between robot and intestinal wall can be easily adjusted by air pressure and air volume. Therefore, the use of airbag expansion to drive three traction modules to adapt to different intestinal diameters can have both the efficiency of caterpillar-track robot and the safety of airbag to a certain extent. However, the airbag and traction module can not be directly combined, and the relative position of the three traction modules should meet the following requirements.

(1) The three traction modules should be symmetrically arranged around the circumference with an interval of 120 degrees.

(2) The airbag should not contact with the intestinal wall as far as possible, otherwise the airbag and the colon will produce friction, which is not conducive to the robot to move forward.

(3) The airbag should also be expandable to increase the deployment diameter of the robot.

Fig.1 show the ABAQUS simulation diagram of the airbag (the air pressure is from -5kPa to 30kPa). The airbag is between the three rods and is bonded with them. In this way, the above three goals can be basically achieved. The 3D model of the robot is shown in Fig. 2(a). Three traction modules are bonded around the airbag. The robot is driven by differential speed like a tank, that is, it can move forward and turn by the speed difference of three tracks. The robot can walk along the colon and turn without the limitation of minimum radius of turning. The robot can adapt to different intestinal diameters by using the balloon expansion.

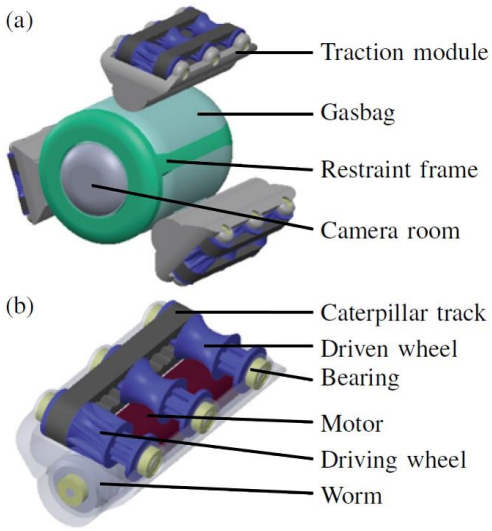

Fig. 2 3D model of the robot. (a) 3D model of the robot in expanded state. (b) 3D model of traction module.

2.3 Design of the traction module

Table 1 Parameters of candidate motors

Gearhead ratio	Runaway speed(rpm)	Stall torque (N · mm)	Length(mm)
700	47	46.12	21.1
136	240	28.57	18.7
26	1200	5.61	16.4

For this scheme, the motor should be parallel to the robot axis. Therefore, there is a 90° power conversion from the motor to the track wheel. It can be seen from Fig. 2(a) that the size of the traction module should gradually increase away from the axis of the robot. Worm gear can achieve this purpose, and it is compact, very suitable for miniaturization design and has large transmission ratio. The 6mm diameter micromotors are used as the power source. There are 3 specifications, as shown in Table I. For routine colonoscopy operation, colonoscopy needs to take 8 minutes to go through the whole colon under the doctor's operation. Therefore, the speed of the robot should not be lower than this speed, i.e. 2.7mm/s. Considering that the robot needs to adjust and stay in the process of moving forward, the speed of the robot should be greater than 3mm/s. As shown in the Fig. 2(b), the traction module should be compact as far as possible, that is, the size should be as small as possible. The motor drives two track wheels in single traction module. The outer diameter of the timing belt pulley is 3mm, the thickness of the timing belt is 1mm, and the part contacting the intestinal wall has a strip pattern with the height of 0.2mm. The driving wheel and driven wheel are printed in 3D, and the spur gear is in the middle of the driving wheels. And the spur gear and driving wheel are integrated. The two driven wheels are thick at both ends and thin in the middle. The middle part is semicircular to prevent interference with the motor, and the middle part can also contact with the intestinal wall to provide certain traction force. Due to the accuracy limitation of 3D printing, in order to ensure the strength of worm gear teeth, the module of worm gear is 0.5mm, the number of teeth is 8 and the number of worm leads is 1. So the speed of the track can be calculated by the following formula.

$$\upsilon_{max} = \frac{\omega_{max}}{N_{\omega}} r \tag{1}$$

Where υ_{max} is the maximum speed of caterpillar track, ω_{max} is the runaway speed of motor, N_{ω} is the reduction ratio of worm gears and r is the radius of track wheel(including track). In Table 1, the

following two types of motors can meet the speed requirements, but in order to ensure that the robot has enough traction, the motor with 136 gearhead ratio is chosen. The final robot prototype is shown in Fig. 3. The dimensions of each part of the robot are shown in table 2. The overall length of the robot is 35mm, and its diameter is 28mm under contraction state. The robot can reach a diameter of more than 50 mm after the airbag is inflated. Although the robot's traction module has a lot of mechanical parts, the weight of the robot is only 14g. In addition, the three rods in the restraint frame can be hollow and the tubes for water insufflation and gas insufflation, biopsy forceps and cable can be placed in them.

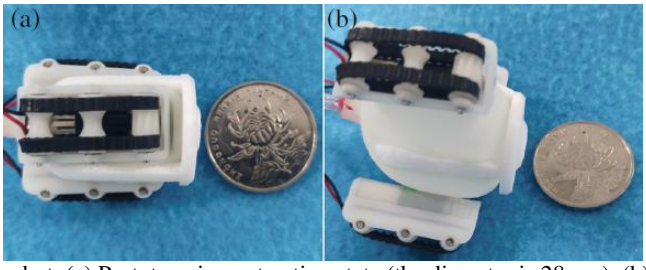

Fig. 3 Prototype of the robot. (a) Prototype in contraction state (the diameter is 28mm). (b) Prototype in expanded state (the diameter is 50mm).

Table 2 Specifications of the fabricated robot

Parameter	Dimension(mm)
Length of the robot	35
Maximum diameter of robot	50
Minimum diameter of robot	28
Length of the traction module	28
Width of the traction module	14
Thickness of the caterpillar track	1
Width of the caterpillar track	2.5
Diameter of the track wheel	3
Diameter of worm gear	6
Modulus of spur gear	0.5
Number of teeth of spur gear	8

3 Output Force Control of The Robot

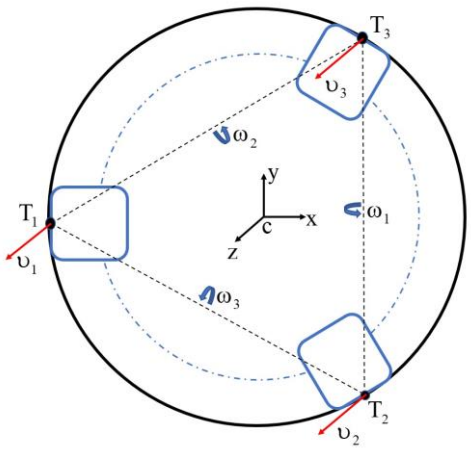

Fig. 4 The axial cross-sectional diagram of the robot.

The output force between the robot track and the intestinal wall needs to be controlled within a certain range. If the output force is too large, the air pressure inside the airbag is too high and the airbag is easy to break. Or the force on the intestinal wall is too large and it will cause damage to the intestinal

tract. If the output force is too small, the robot cannot obtain enough traction force. Next, the statics model and the kinematics model of the airbag will be derived to control the motion and output force of the robot.

3.1 Modelling of kinematics

Kinematics is the basis of robot motion control. For a tracked robot moving in a three-dimensional curved pipeline environment, it has to move forward or backward along the intestinal centerline, and also needs to turn around two axes orthogonal to the tangent of the intestinal axis. In addition, the robot also needs to change its diameter with the change of intestinal diameter. Fig. 4 is the axial cross-sectional diagram of the robot moving in the pipeline. There is a fixed coordinate system {xyz} on the robot, in which the z axis is on the centerline of the robot. T_i (i=1, 2, 3) is the contact center point between the ith(i=1, 2, 3) track module and the intestinal wall on the xcy plane, where T_1 is on the x axis. Several assumptions need to be made.

1) The intestine is regarded as a circular tube.

2) The three track modules are evenly distributed at 120 degrees along the intestinal wall.

3) There is no relative sliding between the track and the intestinal wall.

The velocity of each track module relative to the intestinal wall is υ_i (i=1, 2, 3). In practice, the three velocities coexist with different values. To obtain the contribution of the velocity of each track module to the velocity of the robot, we take the first track module as an example. It is assumed that the velocities of the other two track modules are both zero. υ_1 will make the robot rotate around T_2T_3 with an angular velocity ω_1. According to the geometric relationship, it is easy to obtain:

$$\omega_1 = \frac{\upsilon_1}{0.75d} \tag{2}$$

where d is the diameter of the robot. The components of angular velocity vector $\underline{\omega}_1$ on x axis and y axis are respectively

$$\begin{aligned} \omega_{1x} &= 0 \\ \omega_{1y} &= \frac{\upsilon_1}{0.75d} \end{aligned} \tag{3}$$

Similarly, the velocities of the other two track modules will make the robot rotate around T_1T_3 and T_1T_2. The components of the angular velocity vectors $\underline{\omega}_2$ and $\underline{\omega}_3$ on x axis and y axis are respectively

$$\begin{aligned} \omega_{2x} &= -\frac{\sqrt{3}\upsilon_2}{1.5d} \\ \omega_{2y} &= -\frac{\upsilon_2}{1.5d} \\ \omega_{3x} &= \frac{\sqrt{3}\upsilon_3}{1.5d} \\ \omega_{3y} &= -\frac{\upsilon_3}{1.5d} \end{aligned} \tag{4}$$

υ_i also makes the robot center have a velocity υ_{cz} along the z axis, which satisfies

$$\upsilon_{cz} = \frac{\upsilon_i}{3} \tag{5}$$

Thus, according to the superposition principle, the components of the angular velocity of the robot on the x-axis and Y-axis and the central velocity are

$$\omega_x = -\frac{\sqrt{3}\upsilon_2}{1.5d} + \frac{\sqrt{3}\upsilon_3}{1.5d} \tag{6}$$

$$\omega_y = \frac{2\upsilon_1}{1.5d} - \frac{\upsilon_2}{1.5d} - \frac{\upsilon_3}{1.5d} \tag{7}$$

$$\upsilon_{cz} = \frac{1}{3}(\upsilon_1 + \upsilon_2 + \upsilon_3) \tag{8}$$

Then the relationship between the input velocity of the robot $\upsilon_{in} = \begin{bmatrix} \upsilon_1 & \upsilon_2 & \upsilon_3 \end{bmatrix}^T$ and the velocity output of the robot $\upsilon_{\text{out}} = \begin{bmatrix} \omega_x & \omega_y & \upsilon_{cz} \end{bmatrix}^T$ is

$$\upsilon_{\text{out}} = \left[G_{in}^{\text{out}} \right] \upsilon_{in} \tag{9}$$

where

$$\left[G_{in}^{\text{out}} \right] = \begin{bmatrix} 0 & -\frac{\sqrt{3}}{1.5d} & \frac{\sqrt{3}}{1.5d} \\ \frac{2}{1.5d} & -\frac{1}{1.5d} & -\frac{1}{1.5d} \\ \frac{1}{3} & \frac{1}{3} & \frac{1}{3} \end{bmatrix} \tag{10}$$

If the desired speed output of the robot is given, the speed input of the robot should be

$$\upsilon_{in} = \left[G_{in}^{\text{out}} \right]^{-1} \upsilon_{out} \tag{11}$$

It should be noted that the diameter of the robot d is not determined by the robot. The diameter of the robot is constrained by the size of the intestine. The diameter of the robot should be estimated according to the air pressure and volume in the airbag. Next, the estimation method of robot diameter is described in detail.

3.2 Modelling of statistics

From the view of the mechanism, we should set up a more practicable model for easy and effective realization. For a balloon in the intestinal tract with varying diameter, the contact force between the balloon and the intestine is not only related to the air pressure in the balloon, but also to the inflation volume of the balloon [32]. The robot proposed here is similar to it. In order to make the track output constant force, it is necessary to establish the mechanical model of the robot. As shown in Fig. 5(a) and Fig. 6(a), the airbag of the robot is connected with the cylinder through the air tube, and the air in these three is isolated from the outside, so the ideal gas law is satisfied.

$$PV = nRT \tag{12}$$

Where P is the air pressure inside the air cylinder, air tube and airbag. Although the air pressure inside them will be different in practice, it is assumed that the internal pressure of the three is the same. n is

the mole number of gas, R is the gas constant and T is the temperature in the system, which can be regarded as a constant. V is the sum of internal air volumes of the air cylinder, air tube and airbag.

$$V=V_c+V_t+V_a \tag{13}$$

Here V_c is the air volume in the cylinder, V_t is the air volume in the whole connecting pipe (constant), V_a is the air volume in the airbag. The volume of air in the cylinder can be obtained by the product of piston displacement and piston cross-sectional area. The air volume in the airbag is related to the diameter and air pressure of the robot. The diameter of a robot is the diameter of the smallest circle that can surround all parts of the robot. This can be understood as follows. When the robot is in a pipe, all three groups of tracks contact the inner wall of the pipe. At this time, if the air pressure is increased, the airbag will continue to expand, that is, the air volume in the airbag will become larger. The larger the pipe diameter, the larger the air volume in the airbag. Therefore, V_a is a function of pressure P and pipe diameter d .

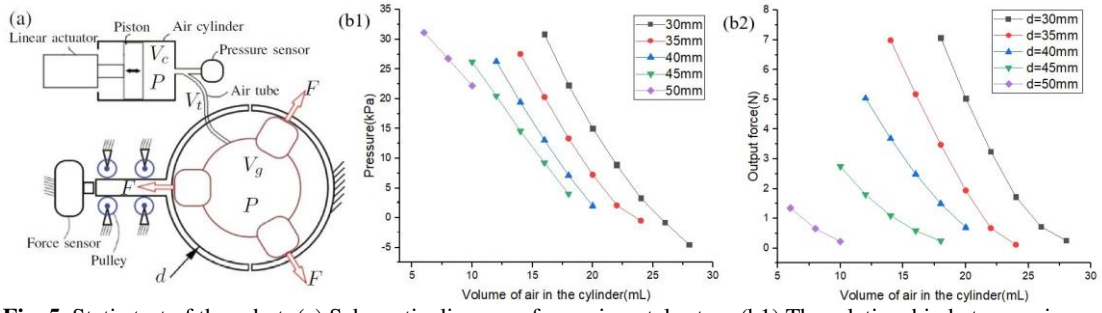

Fig. 5 Static test of the robot. (a) Schematic diagram of experimental setup. (b1) The relationship between air pressure in airbag and air volume in cylinder in different pipes. (b2) The relationship between output force of caterpillar tracks and air volume in cylinder in different pipes.

$$V_a=f_1(P,d) \tag{14}$$

By combining Equation(12), (13) and (14), we can get the following results:

$$P[V_c+V_t+f_1(P,d)] = nRT \tag{15}$$

Then P is the function of V_c and d .

$$P=f_2(V_c, d) \tag{16}$$

Similarly, the higher the air pressure in the airbag, the greater the output force of the track. The output force of the caterpillar track is perpendicular to the axis of the robot. The larger the pipe diameter, the smaller the output force, or even zero. So the output force F is also a function of pressure P and pipe diameter d .

$$F=f_3(P, d) \tag{17}$$

It can be seen by substituting the (16) into (17) that F is a function of V_c and d , so

$$F = f_4(V_c,d) \tag{18}$$

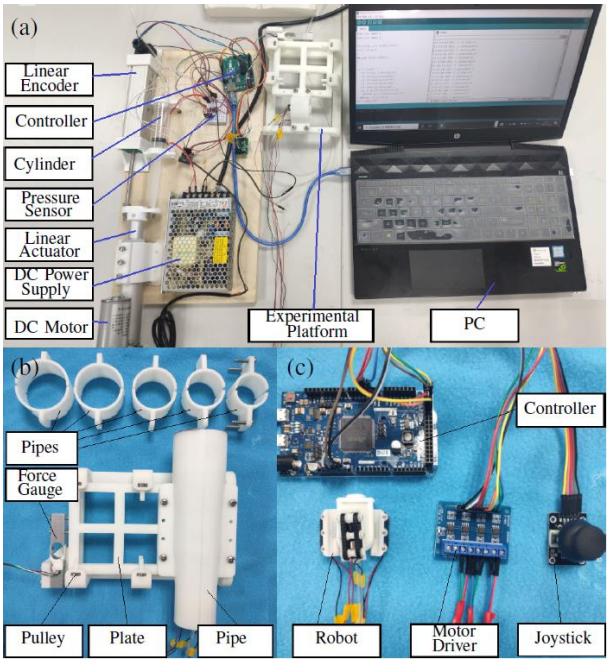

Fig. 6 The test system of the robot. (a) The whole test platform of robot. (b) Output force test bench. (c) Control hardware of robot.

3.2 Characteristics of the robot

It is difficult to get accurate expressions of the above two formulas (6) and (8) through theoretical derivation, but we can get enough accurate expressions through experimental data. As shown in Fig. 5(a) and Fig. 6(b), each 3D-printed pipe is divided into two parts, one half of which is fixed and the other half is fixedly connected with a long plate. The long plate passes through the rows of pulleys through the up, down, left and right sides, one end of which is against the force sensor. In this way, the output force of a single track can be measured. The friction force between the long plate and the pulleys is about 0.035 N, which has negligible influence on the experimental results. When the robot is placed in pipes of different diameters, the air volume in the cylinder is changed, and the pressure curve is shown in Fig. 5(b1). It can be seen from the figure that the air pressure and the air volume in the cylinder meet a certain linearity. And the parallelism of the five relation lines is higher. Similarly, the output positive pressure of the track is shown in Fig. 5(b2). The output force of the track is related to the air pressure in the airbag and the actual contact area between the track and the airbag. When the air pressure reaches a certain value, the actual contact area between the air bag and the airbag almost does not change, and the output force of the track is only related to the air pressure. Therefore, when the air pressure is high, the linearity between the output force and the air in the cylinder is also high. Because the larger the diameter of the pipe is, the smaller the actual contact area between the traction module and the airbag, and the air pressure also needs to overcome the elastic force of the airbag itself, so the output force of the track obviously decreases.

With so many data mentioned above, polynomial can be used to fit the relationship between P, V_c, d and F, V_c, d. In fact, it is necessary to estimate the current diameter of the robot first, because it is of great significance to the motion control of the robot and affects the turning angular velocity of the robot. Therefore, the function of d with respect to P and V_c need to be fit.

$$d = g(P, V_c) \tag{19}$$

The fitting principle is as follows.

$$f(x,y)=\sum_{i=1}^{p}\sum_{j=1}^{q}a_{ij}x^{i-1}y^{j-1} \tag{20}$$

$$s(a_{11},\mathrm{L}\ ,a_{pq})=\sum_{g=1}^{n}w_g(\sum_{i=1}^{p}\sum_{j=1}^{q}a_{ij}x^{i-1}y^{j-1}-z_g)^2 \tag{21}$$

Where $f(x,y)$ is the fitted function, a_{ij} is the coefficient before each term in a polynomial, w_g is weighting coefficient (can be set as 1 here) and z_g is the function value of the actual data point. The purpose is to find a set of coefficients $(a_{11},\mathrm{L}\ ,a_{pq})$ to minimize the function s. The above process can be easily obtained by MATLAB. The final result is that the third order can fit the mathematical relationship of the three accurately. After estimating the diameter of the robot, and then according to the set value of the output force of the robot track, V_c can be calculated, that is, where the piston should be. Therefore, it is necessary to fit the functional relationship of V_c on F and d.

$$V_c=h(F,d) \tag{22}$$

Similarly, using MATLAB to get d for the third order, F for the second order, we can accurately fit the function relationship.

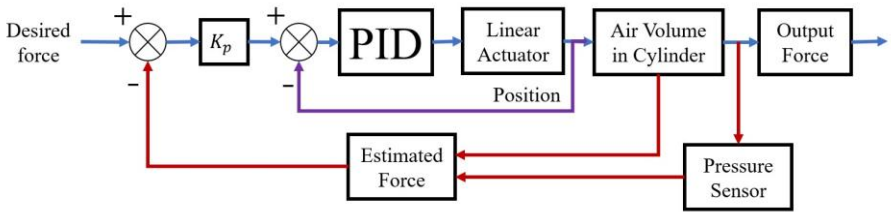

Fig. 7 Control algorithm of robot output force.

3.3 Control Method

The forward speed of the robot is slow, so the diameter of the robot changes slowly. The expansion of the robot airbag can be regarded as a quasi-static process, that is, the air pressure in the airbag is the same as that in the cylinder. Therefore, the statics model mentioned above can be used as the control basis of the robot. The volume of air in the cylinder is the only quantity that can be directly controlled. In addition, there is the feedback quantity of air pressure. Firstly, the diameter of the robot is estimated according to the formula (9), and then according to the estimated diameter and the set value of the robot track output force, the air volume in the cylinder can be obtained by using the formula (12). The control law is shown in Fig. 7, in which the stroke of linear actuator is controlled by PID. The error between the force set value and the estimated value is converted into the ideal position and enters the position control loop. The control frequency of PID inner loop is far greater than that of outer loop.

4 Experiments

4.1 Effect of force control

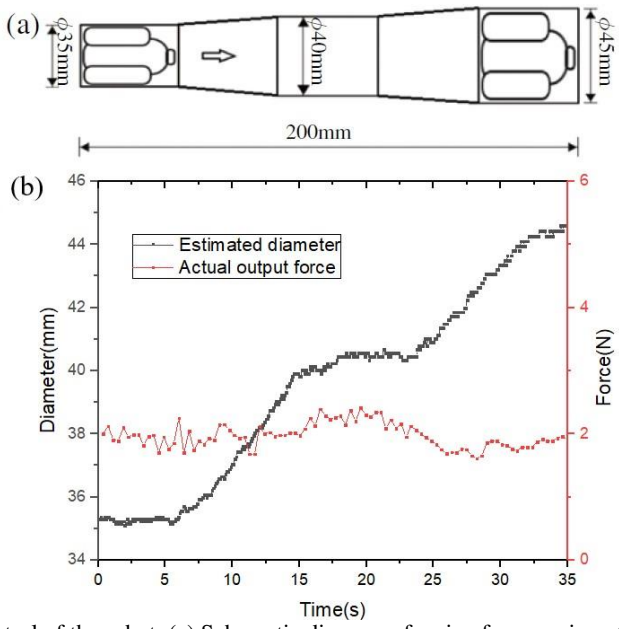

Fig. 8 Output force control of the robot. (a) Schematic diagram of a pipe for experimental testing with changing diameters. (b) The estimated pipe diameter and the actual output force of the track during the experiment.

In order to test the effect of force control, a pipe with variable diameter is selected to test the force control performance of the robot. As shown in Fig. 6(b) and Fig. 8(a), the pipe (the one on the bench in Fig. 6(b)) is 200mm long, which is divided into 5 sections, equal diameter sections of 35mm, 40mm and 45mm, and two transition sections connecting the three. The installation method is similar to the statics experiment. The robot runs from one end of the pipe to the other. Since the forward speed of the robot can not be guaranteed to be constant, it is impossible to know the state of the robot at a specific point in the pipeline. However, the whole running time of the robot can be measured. According to the [7], the output force of the track of the robot should be greater than 0.66N. In this experiment, the value is set to 2N. In this process, according to the air volume and air pressure state in the cylinder, the estimated pipe diameter of the controller is shown in Fig. 8(b). It can be seen that the estimation error of the three equal diameter pipe sections is less than 1mm, and the estimation effect of the two transition sections is also very optimistic. Similarly, during this period, the robot track output force measured by the force sensor is also shown in Fig. 8(b), and the actual maximum error is about 0.4N. The main causes of the error are as follows.

(1) The mechanical model is not accurate enough.

(2) The whole process is not completely quasi-static, that is, the air pressure in the air bag and the cylinder is different.

(3) In the process of robot movement, the measured track is not always aligned with the force sensor. That is, the force sensor measures the component force of the track output force.

In short, open-loop control is not as accurate and the actual output force of the robot measured is not so accurate. However, the control effect of track output positive pressure is still acceptable.

4.2 Motion of the robot

In order to prove the feasibility of the robot structure,firstly the robot's forward speed was tested, and then the robot's forward and turning ability in the curved bellows were verified. Fig. 6(c) shows the control hardware of the robot, including a controller, a motor driver, a joystick (and cylinder system in Fig. 6(a)). As shown in Fig. 9(a), the robot was placed in a soft silicone tube with a inner diameter of 40mm. It took about 60s for the robot to move forward a distance of 300mm, with an average speed of 5mm/s, meeting the requirements mentioned previously. Also in this soft silicone tube, the traction

force of the robot was tested. In fact, the traction force is related to the static friction coefficient and the normal force between the track and the pipe wall, as well as the power of the robot itself. During the test, the maximum traction force of the robot was 3.3N which is greater than the required traction force in [7]. When the maximum traction force was reached, the track had slipped, indicating that the robot's power is more than that.

Next, a bellows with an inner diameter of 40m and an outer diameter of 50mm was used to verify the robot's forward and turning ability. As shown in Fig. 9(b1)-(b6), the minimum radius of curvature of the bellows axis is 55mm. The experimental results showed that the robot can move forward and turn in the curved bellows. It took about 95 seconds for robot to move forward 350mm, and the robot successfully went through the turning corner and continued to move forward. It is worth mentioning that even if the robot was not steered in this process, the robot could move forward and turn adaptively.

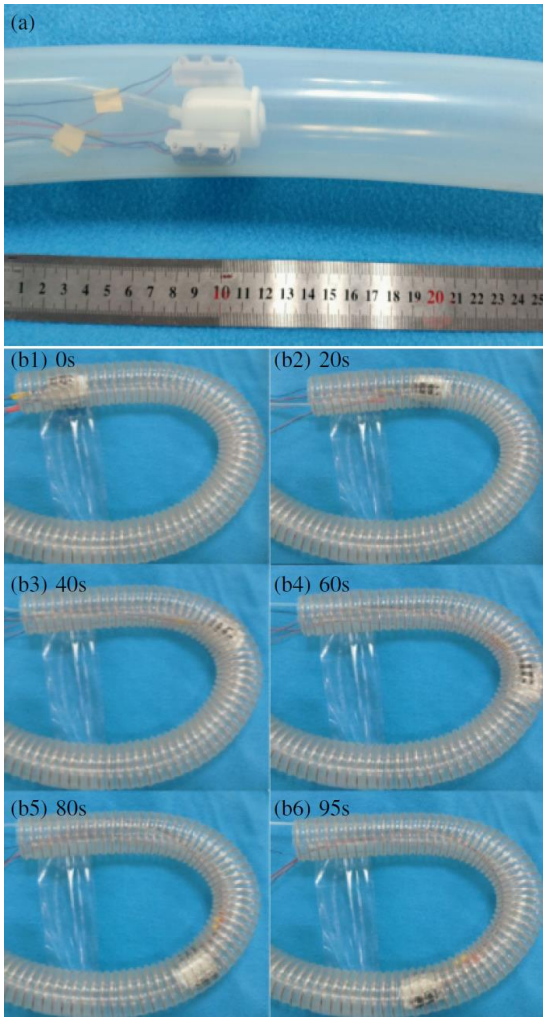

Fig. 9 Experiment of robot locomotion (a) The robot moving in soft silicone tube. (b1)- (b6) Video captures of robot moving in curved bellows.

5 Conclusion

This paper introduces a new type of multi degrees of freedom colon inspection robot which is expanded by airbag. A simple and reliable frame was used to constrain the airbag to keep the robot symmetrical. The whole colon inspection robot is compact and flexible. In addition, the quasi-static mechanical modeling and testing of the robot has been carried out. Taking the statics model fitted by the experimental data as the control basis, the good control effect of the robot track output force was acquired. The traction force and forward speed of the robot were tested by experiments. Moreover, the

forward and turning ability of the robot was verified in the bending bellows. The results showed that the overall performance of the robot is good.

The future work will focus on the motion experiments of the robot in colon model and in vitro animal colon to verify the feasibility of the robot. The driving motor in the proposed robot will be replaced by a 4mm-diameter micromotor. This will make it smaller, easier to pass through the anus the narrow sections of colon. After the completion of these, we will focus on the integration of robot functional devices, such as camera module, waterjet and gas insufflation module and biopsy module.

Acknowledgements
Not applicable.

Author Contributions
JY was in charge of the whole trial and wrote the manuscript; ZS guided the analyses and experiments; YG guided the control of the robot; All authors read and approved the final manuscript.

Author's Information
Jianlin Yang, born in 1995, is currently a PhD student at College of Aerospace Engineering, Nanjing University of Aeronautics and Astronautics, China. His research interest is surgical robotics.
Zhijun Sun, born in 1970, is currently a professor at College of Aerospace Engineering, Nanjing University of Aeronautics and Astronautics, China. His research interest is mechatronics.
Yu Guo, born in 1984, is currently an associate professor at School of Mechanical and Electrical Engineering, Jinling Institute of Technology, China. His research interests include ultrasonic motor application technology and human-interaction robot.

Funding
Supported by National Natural Science Foundation of China (Grant No. 51775274).

Competing Interests
The authors declare no financial competing interests.

Author Details
[1]State Key Laboratory of Mechanics and Control of Mechanical Structures, Nanjing University of Aeronautics and Astronautics, Nanjing 210016, China.[2]College of Mechanical and Electrical Engineering, Jinling Institute of Technology, Nanjing 211169, China.

References

1. Schreuders E H , Ruco A , Rabeneck L , et al. Colorectal cancer screening: a global overview of existing programmes. Gut, 2015, 64(10).
2. Ming L, Olver I , Keefe D , et al. Pre-diagnostic colonoscopies reduce cancer mortality - results from linked population-based data in South Australia. BMC Cancer, 2019, 19.
3. Mateescu B R, Bengus A, Marinescu M, et al. First Pillcam Colon 2 capsule images of Whipple's disease: case report and review of the literature. World J Gastrointest Endosc, 2012, 4(12): 575-578.
4. Sliker L J, Kern M D, Rentschler M E. An Automated Traction Measurement Platform and Empirical Model for Evaluation of Rolling Micropatterned Wheels. IEEE/ASME Transactions on Mechatronics, 2015, 20(4):1854-1862.
5. Nagase J Y, Fukunaga F, Ogawa K, et al. Funicular Flexible Crawler for Colonoscopy. IEEE Transactions on Medical Robotics and Bionics, 2019, 1(1): 22-29.
6. Formosa G A, Prendergast J M, Edmundowicz S A, et al. Novel Optimization-Based Design and Surgical Evaluation of a Treaded Robotic Capsule Colonoscope. IEEE Transactions on Robotics, 2019, 36(2): 545-552.
7. Norton J, Hood A, Neville A, et al. RollerBall: a mobile robot for intraluminal locomotion. In: Proceedings of IEEE International Conference on Biomedical Robotics & Biomechatronics. Qindao: IEEE, 2016, 254-259.

8. Norton. The Design and Development of a Mobile Colonoscopy Robot. Doctoral thesis, 2017.
9. Lee D, Joe S, Choi J, et al. An elastic caterpillar-based self-propelled robotic colonoscope with high safety and mobility. Mechatronics, 2016, 39:54-62.
10. Osawa K, Nakadate R, Arata J, et al. Self-Propelled Colonoscopy Robot Using Flexible Paddle. IEEE Robotics and Automation Letters, 2020, 5(4): 6710-6716.
11. Valdastri P, Webster R J, Quaglia III C, et al. A New Mechanism for Mesoscale Legged Locomotion in Compliant Tubular Environments. IEEE Transactions on Robotics, 2009, 25(5):1047-1057.
12. Dongkyu L, Seonggun J, Kang H, et al. A reel mechanism-based robotic colonoscope with high safety and maneuverability. Surgical Endoscopy, 2018, 33: 322-332.
13. Kwon J, Park S, Park J, et al. Evaluation of the critical stroke of an earthworm-like robot for capsule endoscopes. Proceedings of the Institution of Mechanical Engineers Part H Journal of Engineering in Medicine, 2007, 221(4):397-405.
14. Kang M, Joe S, An T, et al. A novel robotic colonoscopy system integrating feeding and steering mechanisms with self-propelled paddling locomotion: A pilot study. Mechatronics, 2021,73.
15. Manfredi L, Capoccia E, Ciuti G, et al. a soft pneumatic inchworm double balloon (SPID) for colonoscopy. Scientific Reports, 2019, 9:11109.
16. Gao J, Yan G, Wang Z, et al. Design and Testing of a Motor-Based Capsule Robot Powered by Wireless Power Transmission. IEEE/ASME Transactions on Mechatronics, 2016, 21(2):683-693.
17. Heung H L, Chiu P, Zheng L. Design and prototyping of a soft earthworm-like robot targeted for GI tract inspection. In: Proceedings of IEEE International Conference on Robotics and Biomimetics (ROBIO). Qindao: IEEE, 2016, 497-502.
18. Kim B, Lim H Y, Park J H, et al. Inchworm-Like Colonoscopic Robot with Hollow Body and Steering Device. JSME International Journal, 2006, 49(1):205-212.
19. Kim H, Kim J, You J M, et al. A Sigmoid-Colon-Straightening Soft Actuator with Peristaltic Motion for Colonoscopy Insertion Assistance: easyColon. IEEE Robotics and Automation Letters, 2021, 6(2): 3577-3584.
20. Chen Z, Liu J, Wang S, et al. A bio-inspired self-propelling endoscopic device for inspecting the large intestine[J]. Bioinspiration & Biomimetics, 2019, 14(6).
21. Wang K, Wang Z, Zhou Y, et al. Squirm robot with full bellow skin for colonoscopy. In: Proceedings of IEEE International Conference on Robotics & Biomimetics. Tianjin: IEEE, 2010, 53-57.
22. Alcaide J O, Pearson L, Rentschler M E. Design, modeling and control of a SMA-actuated biomimetic robot with novel functional skin. In: Proceedings of IEEE International Conference on Robotics and Automation. Singapore: IEEE, 2017, 4338-4345.
23. Dehghani H, Welch C R, Pourghodrat A, et al. Design and preliminary evaluation of a self-steering, pneumatically driven colonoscopy robot. Journal of Medical Engineering & Technology, 2017, 41(3):223-236.
24. Nelson C A, Dasgupta P, POURGHODRAT A et al. Semi-Autonomous Locomotion for Diagnostic Endoscopy Device. Journal of Medical Devices, 2015, 9(030931): 1-2.
25. Huda M N, Yu H, Shuang C. Robots for minimally invasive diagnosis and intervention. Robotics and Computer Integrated Manufacturing, 2016, 41(OCT.):127-144.
26. Ciuti G, Skonieczna−Zydecka K, Marlicz W, et al. Frontiers of Robotic Colonoscopy: A Comprehensive Review of Robotic Colonoscopes and Technologies[J]. Journal of Clinical Medicine, 2020, 9(6):1648.
27. Natividad R F, Rosario M, Chen P, et al. A hybrid plastic-fabric soft bending actuator with reconfigurable bending profiles. In: Proceedings of IEEE International Conference on Robotics & Automation. Singapore: IEEE, 2017, 6700-6705.

28. Wyatt F. Folded-Tube Soft Pneumatic Actuators for Bending. Soft Robotics, 2019, 6(2): 1-10.
29. Sadahiro S, Ohmura T, Yamada Y, et al. Analysis of length and surface area of each segment of the large intestine according to age, sex and physique. Surg Radiol Anat, 1992,14: 251–257.
30. Sidhu R. Gastrointestinal capsule endoscopy: from tertiary centres to primary care. Bmj, 2006, 332(7540):528-531.
31. Kassim I, Phee L, Ng W S, et al. Locomotion techniques for robotic colonoscopy. IEEE Engineering in Medicine and Biology Magazine, 2006, 25(3):49-56.
32. Poon C C Y, Leung B, Chan C K W, et al. Design of wormlike automated robotic endoscope: dynamic interaction between endoscopic balloon and surrounding tissues. Surgical Endoscopy, 2015, 30(2):772-778.

Supplementary Files

This is a list of supplementary files associated with this preprint. Click to download.

- video.mp4